

New Limits on Axionlike Particle Coupling with the Photons from Two-Photon Decays and Inverse Primakoff Scattering

C.-P. Wu,¹ C.-P. Liu,^{2,3,*} L. Singh,^{4,5} Greeshma C.,⁵ J.-W. Chen,^{6,3,†} H.-C. Chi,² M.K. Pandey,⁶ and H.T. Wong^{4,‡}

¹*Département de Physique, Université de Montréal, Montréal H3C 3J7, Canada.*

²*Department of Physics, National Dong Hwa University, Shoufeng, Hualien 97401, Taiwan.*

³*Physics Division, National Center for Theoretical Sciences, National Taiwan University, Taipei 10617, Taiwan.*

⁴*Institute of Physics, Academia Sinica, Taipei 11529, Taiwan.*

⁵*Department of Physics, School of Physical and Chemical Sciences, Central University of South Bihar, Gaya 824236, India*

⁶*Department of Physics, CTP and LeCosPA, National Taiwan University, Taipei 10617, Taiwan.*

(Dated: June 17, 2022)

Axionlike Particles (ALPs) can be produced in the Sun and is a viable candidate to the Cosmological Dark Matter. It can decay to two photons or interact with matter via Inverse Primakoff (IP) scattering. We identify inelastic channels to the IP-processes due to atomic excitation and ionization. Their cross sections are derived with full electromagnetic fields of atomic charge and current densities, and computed by well-benchmarked atomic many-body methods. Limits on ALP couplings with the photons are derived. New parameter space of ALP masses between 1 eV to 1 MeV not accessible to previous laboratory experiments is probed and excluded. The sensitivity reach in future experimental projects is projected.

PACS numbers: 14.80.Va, 95.35.+d, 13.85.Hd

Keywords: Axions, Dark Matter, Inelastic Scattering

Axions (denoted as a) are hypothetical particles first introduced to solve the strong CP problem with the spontaneous breaking of the Peccei-Quinn symmetry [1–4]. Theoretical and experimental studies later evolve from the original “QCD axions” to variants generically called “axionlike particles” (ALPs), whose masses and coupling strengths with matter are no longer related.

The interaction Lagrangian of an ALP field (ϕ_a) with a photon field (strength tensor as $F_{\mu\nu}$) and Standard-Model fermion fields (Ψ_f , with mass m_f) is generally written as [5]

$$\mathcal{L}_I = -\frac{g_{a\gamma\gamma}}{4}\phi_a F_{\mu\nu}\tilde{F}^{\mu\nu} - \sum_f \frac{g_{aff}}{2m_f}\partial_\mu\phi_a\bar{\Psi}_f(\gamma^\mu\gamma_5)\Psi_f, \quad (1)$$

where $\tilde{F}^{\mu\nu} \equiv \frac{1}{2}\epsilon^{\mu\nu\rho\sigma}F_{\rho\sigma}$ with $\epsilon^{0123}=1$, and $g_{a\gamma\gamma}$ (g_{aff}) denotes the strength of ALP-photon (ALP-fermion) coupling. These interaction terms are the foundation of ALP detection and production.

Sources of ALPs are diverse: they are well-motivated dark matter (DM) candidates, and can be produced in astrophysical environments and terrestrial laboratories. Measureable signatures also cover a wide variety of setups including micro-wave cavities, solar-ALP helioscopes; indirect searches of anomalous electromagnetic radiations in the universe, as well as constraints from cooling of astrophysical objects; and production by colliders or strong laser (see recent reviews [5–9] and references therein).

Data from the DM direct search experiments can place constraints to $g_{a\gamma\gamma}$ and g_{aff} . Through the axio-electric effect, competitive bounds on the ALP-electron coupling g_{aee} have been set in $40 \text{ eV} < m_a < \mathcal{O}(1 \text{ MeV})$ for DM-ALPs, and in a smaller mass range with solar-ALPs (see Ref. [10]). Laboratory constraints on $g_{a\gamma\gamma}$, however, are

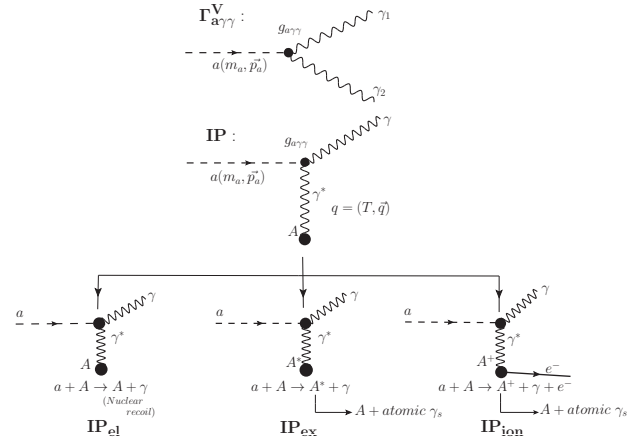


FIG. 1. Schematic diagrams of ALP two-photon decay in vacuum ($\Gamma_{a\gamma\gamma}^V$) and the three IP scattering channels in matter, where kinematics allows one of the photons to be virtual.

comparatively scarce. So far, they are primarily derived from Bragg scattering of solar-ALPs on crystal targets, and only applicable to $m_a < \mathcal{O}(1 \text{ keV})$ [11–15]. The main goal of this work is to expand and improve on the limits in m_a - $g_{a\gamma\gamma}$ space.

The coupling $g_{a\gamma\gamma}$ can manifest experimentally as ALP two-photon decays in vacuum

$$a \rightarrow \gamma_1 + \gamma_2 \quad : \quad \Gamma_{a\gamma\gamma}^V = \frac{1}{64\pi} g_{a\gamma\gamma}^2 m_a^3, \quad (2)$$

where m_a is its mass and $\Gamma_{a\gamma\gamma}^V$ is the decay rate at rest per ALP. Four detection channels for $g_{a\gamma\gamma}$ are shown schematically in Figure 1. When one of the photons becomes virtual in a medium and is absorbed by the target atom A , it gives rise to the Inverse Primakoff (IP) scatter-

ing [16–23] at four-momentum transfer $q_\mu \equiv (T, \vec{q})$. There are three IP reaction channels: $a+A \rightarrow$

$$\left\{ \begin{array}{ll} \gamma + A & \text{IP}_{el} : \text{elastic scattering} \\ \gamma + A^* & \text{IP}_{ex} : \text{atomic excitation} \\ \gamma + A^+ + e^- & \text{IP}_{ion} : \text{atomic ionization} \end{array} \right. \quad (3)$$

All four channels involve full conversion or absorption of the ALPs so that the experimental measurables are the total energy at E_a . There are no interferences among them, since all have experimentally distinguishable final states – two γ s for $\Gamma_{a\gamma\gamma}^V$, a single γ for IP_{el} , γ plus atomic de-excitation photons for IP_{ex} , and γ plus electron with atomic transition photons for IP_{ion} . At m_a much lower than the nucleus mass scales (GeV), the energy depositions at detectors are electromagnetic without complications on their nuclear recoil response.

Existing theoretical studies of IP processes focus on elastic scattering of ALPs by the Coulomb field of a target [16–22]. The inclusive sum of all inelastic scattering channels by solar-ALP was recently estimated in Ref. [23] using the inelastic atomic charge form factor. We advance further in this work by systematically studying the three IP channels via well-benchmarked atomic many-body calculations. The axion velocity and total energy are denoted by, respectively, v_a and $E_a = m_a / \sqrt{1 - v_a^2}$ (both in natural units). Detection of both solar- ($v_a \sim 1$) and DM-ALPs ($v_a \sim 10^{-3}$) are considered.

The transverse electromagnetic field of the target atom is studied for the first time. We identify that, to be elaborated in what follows, the transverse channel dominates the IP_{ion} cross section for DM-ALP. Consequently, the experimental observable is a peak at $E_a \simeq m_a$ in which both electron and photon have equal energy at $E_a/2$. This distinct signature offers the prospects of smoking-gun identification, so that $g_{a\gamma\gamma}$ can be probed with good sensitivity at m_a above detector thresholds.

The evaluation of the double differential cross sections of the ALP IP processes builds on our earlier work of incorporating the atomic many-body physics effects to low energy neutrino [24–26] and DM [27, 28] interactions with matter:

$$\frac{d^2\sigma}{dTd\Omega} = \frac{\alpha_{em} g_{a\gamma\gamma}^2}{16\pi} \frac{E_a - T}{v_a E_a} \left(\frac{V_L}{(q^2)^2} \mathcal{R}_L + \frac{V_T}{(Q^2)^2} \mathcal{R}_T \right), \quad (4)$$

where α_{em} is the fine structure constant, q^2 and $Q^2 = T^2 - q^2$ are the three- and four-momentum transfer squared, respectively. The full unpolarized atomic response consists of the longitudinal and transverse components, \mathcal{R}_L and \mathcal{R}_T , both being functions of T and q^2 and given by:

$$\mathcal{R}_{L/T} = \sum_F \sum_I |\langle F | \rho / \vec{j}_\perp | I \rangle|^2 \delta(E_I - E_F - T), \quad (5)$$

which arise from the charge ρ and transverse current density \vec{j}_\perp , respectively. The initial state $|I\rangle$ corresponds to

the ground state of the target atom, while the choice of final state $|F\rangle$ depends on the IP interaction channels: ground state, excited states and the continuum for IP_{el} , IP_{ex} and IP_{ion} , respectively.

To fully exhibit the pole structure of the photon propagator, which is crucial in cross section calculations, the corresponding kinematic factors V_L and V_T are expressed in powers of q^2 and Q^2 , respectively:

$$V_L = 2 [E_a^2 - m_a^2 + (E_a - T)^2] q^2 - (q^2)^2 - (T^2 - 2E_a T + m_a^2)^2, \quad (6)$$

$$V_T = m_a^4 + \frac{Q^2}{2q^2} [(m_a^4 - 4m_a^2 E_a T) + (2m_a^2 + 4E_a^2 - 4E_a T + 2T^2) Q^2 - (Q^2)^2]. \quad (7)$$

The familiar Coulomb pole $q^2=0$ is realized in the longitudinal component only at the forward angle $\theta=0$ under $T=E_a(1-v_a)$. The resulting single pole in $V_L/(q^2)^2$ (that is, as the last term of Eq. 6 vanishes identically at $q^2 \rightarrow 0$) is usually regulated by introducing a detector target-dependent Coulomb screening factor [17, 18, 21, 22, 29]. We point out that this is automatically realized by the neutrality of atoms such that \mathcal{R}_L starts at the order of q^2 , as demonstrated in Table 1 of Ref. [23] for IP_{el} or in the wave function orthogonality in IP_{ex} and IP_{ion} .

The transverse component $V_T/(Q^2)^2$ does exhibit a double pole structure at $Q^2=0$ for finite m_a . The kinematics of the incoming ALP and outgoing photon

$$Q^2 = m_a^2 - 2E_a(E_a - T)(1 - v_a \cos \theta), \quad (8)$$

makes it possible to have Q^2 vary from time-like to space-like as the scattering angle increases at, for example, $v_a \ll 1$, $E_a \approx m_a$ and $T \approx m_a/2$, which are the conditions for non-relativistic DM-ALPs. As the virtual photon is absorbed by the target, the kinematics of the target final state further limits the available Q^2 -space. In general, $Q^2 \leq 0$ for IP_{el} , and can be both space- and time-like for IP_{ex} and IP_{ion} .

To regulate the transverse photon pole, we improve the approach of Ref. [30] by modifying the photon propagator according to the complex refractive index of the detector materials. This results in a change in Eq. (4) via

$$\frac{1}{(Q^2)^2} \rightarrow \frac{1}{(Q^2 - \Lambda_T^2/4)^2 + T^2 \Lambda_T^2}, \quad (9)$$

where the photon attenuation coefficient $\Lambda_T \equiv n_A \sigma_\gamma(T)$ is expressed in terms of target number density n_A and photo-absorption cross section $\sigma_\gamma(T)$. At T above typical experimental threshold of 100 eV_{ee} (electron-equivalence energy is used to denote detector response), $n_A \sim 10^{22}$ cm⁻³ and $\sigma_\gamma(T) \lesssim 10^6$ barn, so that Λ_T is not larger than a few eV, and $T\Lambda_T \sim (10^2 - 10^4)$ eV². The shift in the pole position is therefore not significant. The real refractive index is taken to be 1, which is a good

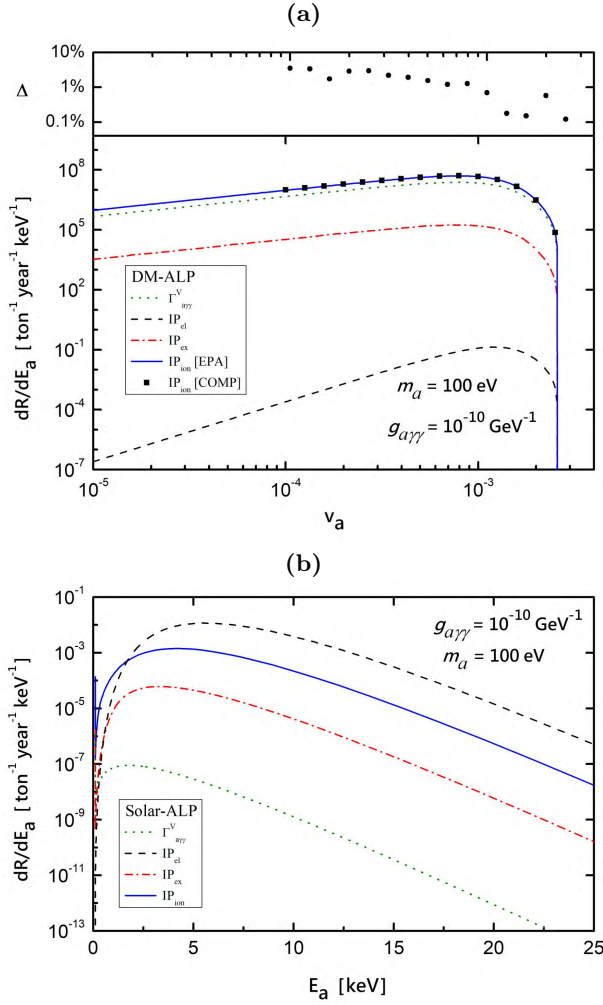


FIG. 2. Differential event rates per ton-year of exposure for the four detection channels in liquid xenon, taking the case of $g_{a\gamma\gamma}=10^{-10}$ GeV $^{-1}$ and $m_a=100$ eV as illustration: (a) DM-ALPs as function of v_a , with the fractional deviations Δ between EPA and COMP calculations for IP_{ion} ; (b) Solar-ALPs versus total energy E_a – the spikes at low E_a correspond to the kinematic regime where the ALPs are non-relativistic.

approximation for X- and γ -ray photons. Refined treatments of photons at lower and near-resonance energies are subjects of future studies.

Evaluation of the transverse contribution for IP_{ion} can be simplified with an equivalent photon approximation (EPA) similar to that of Ref. [30], via: (i) setting $V_L=0$, (ii) keeping only the terms with m_a^4 in V_T of Eq. 7, and (iii) substituting the transverse response $\mathcal{R}_T(T, q)$ by the photo-absorption cross section $\mathcal{R}_T(T, q) \approx T \sigma_\gamma(T) / (2\pi^2 \alpha_{em})$. Eq. 4 can then be integrated to give the single differential cross section (SDCS),

TABLE I. Event rates of the four detection channels in liquid xenon for DM- and solar-ALPs, at $g_{a\gamma\gamma}=10^{-10}$ GeV $^{-1}$. Vacuum decay $\Gamma_{a\gamma\gamma}^V$ is evaluated from Eq. 2, while the three IP channels follow Eq. 5 with different final states $|F\rangle$. For IP_{ex} , only the dominant final states by electric dipole excitations are included.

Event Rates (ton $^{-1}$ year $^{-1}$)				
Detection Channels				
m_a	$\Gamma_{a\gamma\gamma}^V$	IP_{el}	IP_{ex}	IP_{ion}
DM-ALP				
1 eV	2.5×10^{-4}	$\mathcal{O}(10^{-14})$	0	0
1 keV	250	1.7×10^{-5}	1.6×10^{-3}	500
1 MeV	2.5×10^8	9.9×10^{-5}	2.2×10^{-10}	5.0×10^8
solar-ALP				
1 meV	$\mathcal{O}(10^{-27})$	7.0×10^{-2}	2.9×10^{-4}	8.1×10^{-3}
1 eV	$\mathcal{O}(10^{-15})$	7.0×10^{-2}	2.9×10^{-4}	8.1×10^{-3}
1 keV	3.9×10^{-3}	7.0×10^{-2}	2.9×10^{-4}	1.6×10^{-2}

in which the leading order contribution for IP_{ion} is:

$$\left[\frac{d\sigma}{dT} \right]_{EPA}^{IP_{ion}} = \frac{g_{a\gamma\gamma}^2 \sigma_\gamma m_a^4}{32\pi^2 \Lambda_T v_a^2 E_a^2} \tan^{-1} \left[\frac{Q^2 - \Lambda_T^2/4}{T\Lambda_T} \right] \Big|_{Q_{min}^2}^{Q_{max}^2}. \quad (10)$$

The $1/\Lambda_T$ dependence is the consequence of the linear divergence resulting from the double pole. Together with σ_γ , it leads to a SDCS suppression by $1/n_A$. In addition, the factor $m_a^4/(v_a^2 E_a^2) = m_a^2(1-v_a^2)/v_a^2$ favors IP_{ion} cross sections by non-relativistic ($v_a \ll 1$) ALPs of large m_a . Furthermore, the \tan^{-1} value approaches π when $|Q^2| \gg T\Lambda_T$ at its extrema. In such cases, the SDCS is a T -independent constant, bounded by $T \sim m_a(1 \pm v_a)/2$ for non-relativistic $v_a \ll 1$.

The case of $g_{a\gamma\gamma}=10^{-10}$ GeV $^{-1}$ and $m_a=0.1$ keV in liquid xenon detectors is used as illustration. Depicted in Figures 2a&b are the differential event rates of the four detection channels per ton-year exposure for, respectively, two sources: (i) relic DM-ALPs with flux given by the standard halo model [31] with: $v_0=220$ km s $^{-1}$, $v_E=232$ km s $^{-1}$, $v_{esc}=544$ km s $^{-1}$, and $\rho_\chi=0.3$ GeV cm $^{-3}$, and (ii) solar-ALPs with flux given by the Primakoff production in the Sun [32].

In the case of DM-ALPs in Figure 2a, the ratio of differential rates between IP_{ion} and $\Gamma_{a\gamma\gamma}^V$ is about 2 while $T \sim m_a(1 \pm v_a)/2$. The origin is that IP_{ion} and $\Gamma_{a\gamma\gamma}^V$ differ only in their different final states. Two real photons are emitted in $\Gamma_{a\gamma\gamma}^V$ while, as shown by the pole structure of Eq. 9, the target in IP_{ion} can absorb one of the emitted photons as virtual intermediate states. The fractional deviations Δ ($\equiv |IP_{ion}[EPA] - IP_{ion}[COMP]| / IP_{ion}[COMP]$) of the dominant IP_{ion} channel in DM-ALP between EPA and complete (COMP) calculations at several selected values of m_a are depicted as the black data points, demonstrating EPA is a valid description to an accuracy of $<3\%$.

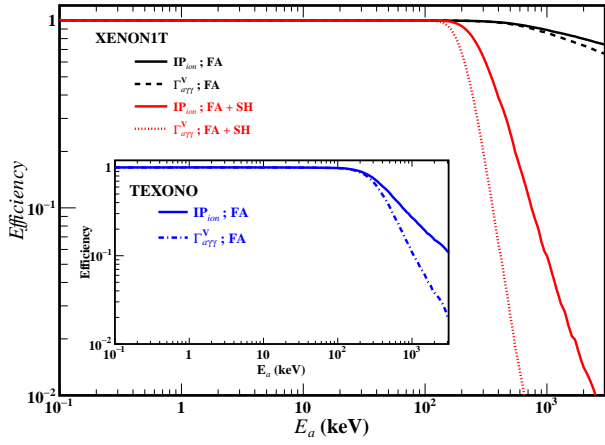


FIG. 3. Signal detection efficiency for DM-ALPs for the leading $\Gamma_{a\gamma\gamma}^V$ and IP_{ion} channels as function of E_a in XENON1T [35] and TEXONO [34] (inset) experiments. Efficiencies due to full absorption (FA) are applicable to both experiments, while single-hit (SH) selection applies in addition to XENON1T. Signatures for solar-ALPs are below 20 keV_{ee} , and the efficiency is close to unity.

Summarized in Table I are the integral event rates for DM- and solar-ALPs at different m_a 's, taking $g_{a\gamma\gamma} = 10^{-10} \text{ GeV}^{-1}$ as illustration. The cross sections of the four channels all vary with $g_{a\gamma\gamma}^2$ while the solar-ALP flux has an additional $g_{a\gamma\gamma}^2$ -dependence in its production. DM-ALPs are non-relativistic. The leading channel is IP_{ion} above the ionization threshold (12 eV_{ee} for Xe) in which the SDCS varies as m_a^2 from Eq. 10 while the total cross section scales with m_a^3 . $\Gamma_{a\gamma\gamma}^V$ is the sub-leading channel with half the rates, and becomes the leading one below the IP_{ion} threshold. Conversely, solar-ALPs are mostly relativistic. The leading channel is IP_{el} and insensitive to m_a . Contributions by $\Gamma_{a\gamma\gamma}^V$ are negligible, suppressed by time dilation and other factors.

The following data sets are adopted for analysis to derive constraints on the $(m_a, g_{a\gamma\gamma})$ plane:

1. TEXONO data with (a) point-contact germanium detector at $300 \text{ eV}_{ee} - 12 \text{ keV}_{ee}$ [33], and (b) high-purity germanium detector at 12 keV_{ee} to 3000 keV_{ee} [34], selected for having both low threshold and high energy (MeV_{ee}) reach yet with detectors of excellent energy resolution (1.98 keV_{ee} at 1 MeV_{ee}) for spectral peak detection.
2. XENON1T “S2-only” data with liquid xenon at $1.5 - 207 \text{ keV}_{ee}$ [35, 36], selected for its large exposure while having low threshold and background. The background is well-modelled and understood, and is subtracted for ALP searches.

The DM-ALPs are non-relativistic and interact predominantly via the $\Gamma_{a\gamma\gamma}^V$ and IP_{ion} channels, the signatures of which are Gaussian peaks at m_a on the total energy depositions over the continuum background spectra.

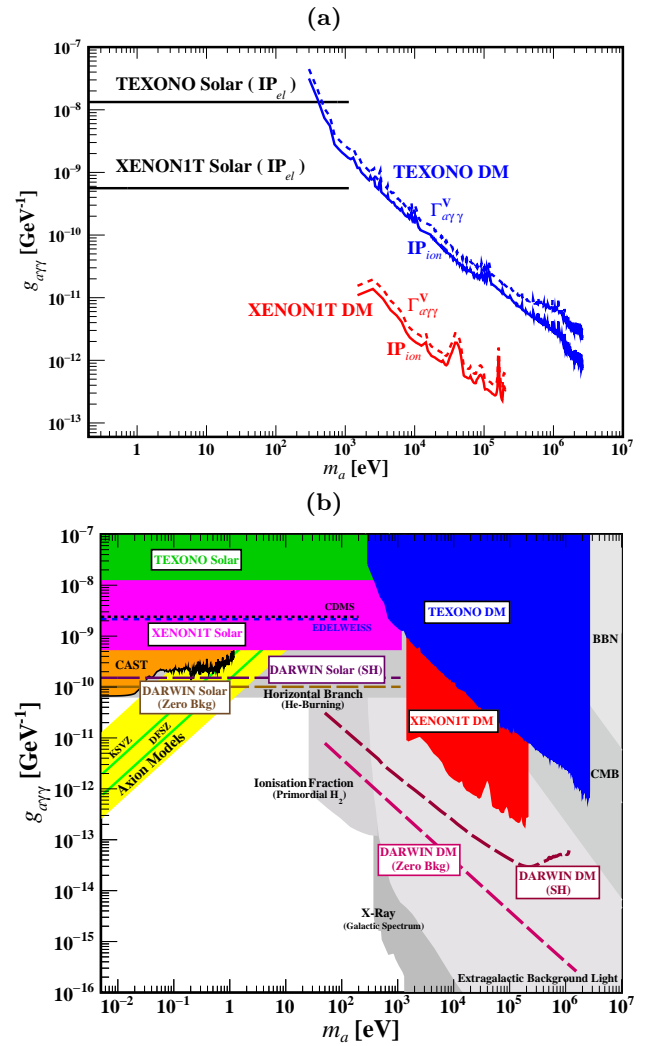


FIG. 4. Exclusion plot in $(m_a, g_{a\gamma\gamma})$ at 90% CL, showing the solar-ALP and DM-ALP bounds from TEXONO [33, 34] and XENON1T [35, 36] experiments. For DM-ALPs, (a) $\Gamma_{a\gamma\gamma}^V$ and IP_{ion} are presented separately in (a) and as combined limits in (b). The astrophysical bounds [7, 37] are the light shaded regions in (b), while the predicted bands for QCD axions [38] are in yellow. Superimposed are the current constraints from solar-ALPs with Bragg scattering [14, 15] and helioscope [39] experiments, as well as the sensitivity reaches of the DARWIN project [40] at standard SH-selection and zero-background scenarios.

Current DM data focuses on “single-hit” events uncorrelated to veto signals from other detector components. Signal efficiencies of having final-state emissions with full absorption (FA) in the detectors and tagged as single-hit (SH) events have to be evaluated. These differ among the two channels with their different final-states: $\Gamma_{a\gamma\gamma}^V$ is with both γ 's each having energy of $E_a/2$; while IP_{ion} has an electron and a photon each at $E_a/2$. In the case of liquid xenon detector, this requirement implies that the final states are fully absorbed within a distance corresponding to the spatial resolution ($\sigma_{x,y} = 0.8 \text{ cm}$ and

$\sigma_z=0.3$ cm at 1 MeV_{ee} [36]) away from the vertices. The energy dependence of signal efficiencies in both channels are depicted in Figure 3. For solar-ALPs which are relativistic, IP_{el} with a one-photon final state is the dominant channel. Signatures are continuous distributions with the ALP spectra convoluted with IP_{el} cross sections. Signal efficiency for single-hit data selection is close to unity at this low (<20 keV_{ee}) energy.

With detection efficiencies taken into account, the exclusion regions at 90% confidence level (CL) of the leading channels ($\Gamma_{a\gamma\gamma}^V$ and IP_{ion} for DM-ALP and IP_{el} for solar-ALP) from the TEXONO and XENON1T experiments are presented in Figure 4a. The solar-ALP constraints and the combined limits of both detection channels for DM-ALPs are displayed in Figure 4b, together with astrophysical bounds [7, 37] and predictions from QCD-axion models [38]. The IP_{el} channel with solar-ALPs improves on $g_{a\gamma\gamma}$ over the Bragg-scattering constraints from CDMS [14] and EDELWEISS [15]. It also extends m_a range to be probed from 1 eV to $\mathcal{O}(\text{keV})$ beyond the reach of the CAST helioscope experiment [39]. In DM-ALP searches, new regions not accessible to other laboratory experiments in $\mathcal{O}(\text{keV}) < m_a < \mathcal{O}(\text{MeV})$ are probed and excluded by IP_{ion} and $\Gamma_{a\gamma\gamma}^V$.

The leading IP_{ion} channel in DM-ALP searches offers very distinct signatures: an electron and a photon with equal energy originated from a common vertex. This can be used for further background suppression while retaining good signal efficiency. The projected sensitivities of the next generation liquid xenon project DARWIN [40] at 200 ton-year exposure and 50 eV_{ee} threshold are superimposed in Figure 4b, showing one with typical single-hit selection with the projected background subtracted, and another with an idealized zero-background all-multiplicity measurement.

This work was supported in part under Contracts 106-2923-M-001-006-MY5, 110-2112-M-001-029-MY3, 108-2112-002-003-MY3, 109-2112-M-259-001 and 110-2112-M-259-001 from the Ministry of Science and Technology, 2019-20/ECP-2 and 2021-22/TG2.1 from the National Center for Theoretical Sciences, and the Kenda Foundation (J.-W. C.) of Taiwan; Contract F.30-584/2021(BSR), UGC-BSR Research Start Up Grant, India (L.S.); and the Canada First Research Excellence Fund through the Arthur B. McDonald Canadian Astroparticle Physics Research Institute (C.-P. W.).

* cpliu@mail.ndhu.edu.tw

† jwc@phys.ntu.edu.tw

‡ ht Wong@phys.sinica.edu.tw

[1] R. D. Peccei and H. R. Quinn, CP Conservation in the Presence of Instantons, *Phys. Rev. Lett.* **38**, 1440 (1977).
 [2] R. D. Peccei and H. R. Quinn, Constraints Imposed by CP Conservation in the Presence of Instantons, *Phys.*

Rev. D **16**, 1791 (1977).
 [3] S. Weinberg, A New Light Boson?, *Phys. Rev. Lett.* **40**, 223 (1978).
 [4] F. Wilczek, Problem of Strong P and T Invariance in the Presence of Instantons, *Phys. Rev. Lett.* **40**, 279 (1978).
 [5] P. A. Zyla *et al.* (Particle Data Group), Review of Particle Physics, *PTEP* **2020**, 083C01 (2020), review 90 by A. Ringwald, L.J. Rosenberg and G. Rybka.
 [6] P. W. Graham, I. G. Irastorza, S. K. Lamoreaux, A. Lindner, and K. A. van Bibber, Experimental Searches for the Axion and Axion-Like Particles, *Ann. Rev. Nucl. Part. Sci.* **65**, 485 (2015), arXiv:1602.00039 [hep-ex].
 [7] I. G. Irastorza and J. Redondo, New experimental approaches in the search for axion-like particles, *Prog. Part. Nucl. Phys.* **102**, 89 (2018), arXiv:1801.08127 [hep-ph].
 [8] P. Sikivie, Invisible Axion Search Methods, *Rev. Mod. Phys.* **93**, 015004 (2021), arXiv:2003.02206 [hep-ph].
 [9] K. Choi, S. H. Im, and C. Sub Shin, Recent Progress in the Physics of Axions and Axion-Like Particles, *Ann. Rev. Nucl. Part. Sci.* **71**, 225 (2021), arXiv:2012.05029 [hep-ph].
 [10] C. O'Hare, cajohare/axionlimits: Axionlimits, <https://cajohare.github.io/AxionLimits/> (2020).
 [11] F. T. Avignone, III *et al.* (SOLAX), Experimental search for solar axions via coherent Primakoff conversion in a germanium spectrometer, *Phys. Rev. Lett.* **81**, 5068 (1998), arXiv:astro-ph/9708008.
 [12] R. Bernabei *et al.*, Search for solar axions by Primakoff effect in NaI crystals, *Phys. Lett. B* **515**, 6 (2001).
 [13] A. Morales *et al.* (COSME), Particle dark matter and solar axion searches with a small germanium detector at the Canfranc Underground Laboratory, *Astropart. Phys.* **16**, 325 (2002), arXiv:hep-ex/0101037.
 [14] Z. Ahmed *et al.* (CDMS), Search for Axions with the CDMS Experiment, *Phys. Rev. Lett.* **103**, 141802 (2009), arXiv:0902.4693 [hep-ex].
 [15] E. Armengaud *et al.*, Axion searches with the EDELWEISS-II experiment, *JCAP* **1311**, 067, arXiv:1307.1488 [astro-ph.CO].
 [16] S. Barshay, H. Faissner, R. Rodenberg, and H. De Witt, Coherent Conversion of Very Light Pseudoscalar Bosons, *Phys. Rev. Lett.* **46**, 1361 (1981).
 [17] F. T. Avignone, C. Baktash, W. C. Barker, F. P. Calaprice, R. W. Dunford, W. C. Haxton, D. Kahana, R. T. Kouzes, H. S. Miley, and D. M. Moltz, Search for Axions From the 1115-keV Transition of ^{65}Cu , *Phys. Rev. D* **37**, 618 (1988).
 [18] W. Buchmuller and F. Hoogeveen, Coherent Production of Light Scalar Particles in Bragg Scattering, *Phys. Lett. B* **237**, 278 (1990).
 [19] E. A. Paschos and K. Zioutas, A Proposal for solar axion detection via Bragg scattering, *Phys. Lett. B* **323**, 367 (1994).
 [20] R. J. Creswick, F. T. Avignone, III, H. A. Farach, J. I. Collar, A. O. Gattone, S. Nussinov, and K. Zioutas, Theory for the direct detection of solar axions by coherent Primakoff conversion in germanium detectors, *Phys. Lett. B* **427**, 235 (1998), arXiv:hep-ph/9708210.
 [21] J. B. Dent, B. Dutta, J. L. Newstead, and A. Thompson, Inverse Primakoff Scattering as a Probe of Solar Axions at Liquid Xenon Direct Detection Experiments, *Phys. Rev. Lett.* **125**, 131805 (2020), arXiv:2006.15118 [hep-ph].
 [22] C. Gao, J. Liu, L.-T. Wang, X.-P. Wang, W. Xue, and

- Y.-M. Zhong, Reexamining the Solar Axion Explanation for the XENON1T Excess, *Phys. Rev. Lett.* **125**, 131806 (2020), [arXiv:2006.14598 \[hep-ph\]](#).
- [23] T. Abe, K. Hamaguchi, and N. Nagata, Atomic Form Factors and Inverse Primakoff Scattering of Axion, *Phys. Lett. B* **815**, 136174 (2021), [arXiv:2012.02508 \[hep-ph\]](#).
- [24] J.-W. Chen, H.-C. Chi, K.-N. Huang, C.-P. Liu, H.-T. Shiao, L. Singh, H. T. Wong, C.-L. Wu, and C.-P. Wu, Atomic ionization of germanium by neutrinos from an ab initio approach, *Phys. Lett. B* **731**, 159 (2014), [arXiv:1311.5294 \[hep-ph\]](#).
- [25] J.-W. Chen, H.-C. Chi, H.-B. Li, C.-P. Liu, L. Singh, H. T. Wong, C.-L. Wu, and C.-P. Wu, Constraints on millicharged neutrinos via analysis of data from atomic ionizations with germanium detectors at sub-keV sensitivities, *Phys. Rev. D* **90**, 011301 (2014), [arXiv:1405.7168 \[hep-ph\]](#).
- [26] J.-W. Chen, H.-C. Chi, K.-N. Huang, H.-B. Li, C.-P. Liu, L. Singh, H. T. Wong, C.-L. Wu, and C.-P. Wu, Constraining neutrino electromagnetic properties by germanium detectors, *Phys. Rev. D* **91**, 013005 (2015), [arXiv:1411.0574 \[hep-ph\]](#).
- [27] M. K. Pandey, L. Singh, C.-P. Wu, J.-W. Chen, H.-C. Chi, C.-C. Hsieh, C.-P. Liu, and H. T. Wong, Constraints from a many-body method on spin-independent dark matter scattering off electrons using data from germanium and xenon detectors, *Phys. Rev. D* **102**, 123025 (2020), [arXiv:1812.11759 \[hep-ph\]](#).
- [28] C.-P. Liu, C.-P. Wu, J.-W. Chen, H.-C. Chi, M. K. Pandey, L. Singh, and H. T. Wong, Spin-dependent dark matter-electron interactions, (2021), [arXiv:2106.16214 \[hep-ph\]](#).
- [29] M. C. D. Marsh, The Darkness of Spin-0 Dark Radiation, *JCAP* **01**, 017, [arXiv:1407.2501 \[hep-ph\]](#).
- [30] J.-W. Chen, H.-C. Chi, S.-T. Lin, C.-P. Liu, L. Singh, H. T. Wong, C.-L. Wu, and C.-P. Wu, Atomic ionization by sterile-to-active neutrino conversion and constraints on dark matter sterile neutrinos with germanium detectors, *Phys. Rev. D* **93**, 093012 (2016), [arXiv:1601.07257 \[hep-ph\]](#).
- [31] P. A. Zyla *et al.* (Particle Data Group), Review of Particle Physics, *PTEP* **2020**, 083C01 (2020), review 27 by L. Baudis and S. Profumo, and references therein.
- [32] S. Andriamonje *et al.* (CAST), An Improved limit on the axion-photon coupling from the CAST experiment, *JCAP* **04**, 010, [arXiv:hep-ex/0702006](#).
- [33] L. Singh *et al.* (TEXONO), Constraints on millicharged particles with low threshold germanium detectors at Kuo-Sheng Reactor Neutrino Laboratory, *Phys. Rev. D* **99**, 032009 (2019), [arXiv:1808.02719 \[hep-ph\]](#).
- [34] H. T. Wong *et al.* (TEXONO), A Search of Neutrino Magnetic Moments with a High-Purity Germanium Detector at the Kuo-Sheng Nuclear Power Station, *Phys. Rev. D* **75**, 012001 (2007), [arXiv:hep-ex/0605006](#).
- [35] E. Aprile *et al.* (XENON), Excess electronic recoil events in XENON1T, *Phys. Rev. D* **102**, 072004 (2020), [arXiv:2006.09721 \[hep-ex\]](#).
- [36] E. Aprile *et al.* (XENON), XENON1T Dark Matter Data Analysis: Signal Reconstruction, Calibration and Event Selection, *Phys. Rev. D* **100**, 052014 (2019), [arXiv:1906.04717 \[physics.ins-det\]](#).
- [37] D. Cadamuro and J. Redondo, Cosmological bounds on pseudo Nambu-Goldstone bosons, *JCAP* **02**, 032, [arXiv:1110.2895 \[hep-ph\]](#).
- [38] G. G. Raffelt, Axions: Motivation, limits and searches, *J. Phys. A* **40**, 6607 (2007), [arXiv:hep-ph/0611118](#).
- [39] V. Anastassopoulos *et al.* (CAST), New CAST Limit on the Axion-Photon Interaction, *Nature Phys.* **13**, 584 (2017), [arXiv:1705.02290 \[hep-ex\]](#).
- [40] J. Aalbers *et al.* (DARWIN), DARWIN: towards the ultimate dark matter detector, *JCAP* **11**, 017, [arXiv:1606.07001 \[astro-ph.IM\]](#).